# *Late gene therapy limits the restoration of retinal function in a mouse model of retinitis pigmentosa*

Miranda L. Scalabrino*[1,2], Mishek Thapa*[1,2], Tian Wang[3], Alapakkam P. Sampath[1], Jeannie Chen[3], Greg D. Field[1,2]

1. Stein Eye Institute, Department of Ophthalmology, University of California, Los Angeles CA
2. Department of Neurobiology, Duke University School of Medicine, Durham NC
3. Zilkha Neurogenetic Institute, Keck School of Medicine, University of Southern California, Los Angeles CA

* authors contributed equally

### *Abstract*

Retinitis pigmentosa is an inherited photoreceptor degeneration that begins with rod loss followed by cone loss and eventual blindness. Gene therapies are being developed, but it is unknown how retinal function depends on the time of intervention. To uncover this dependence, we utilized a mouse model of retinitis pigmentosa capable of artificial genetic rescue. This model enables a benchmark of best-case gene therapy by removing the variables that complicate the ability to answer this vital question. Complete genetic rescue was performed at 25%, 50%, and 70% rod loss (early, mid and late, respectively). Early and mid treatment restored retinal function to near wild-type levels, specifically the sensitivity and signal fidelity of retinal ganglion cells (RGCs), the 'output' neurons of the retina. However, some anatomical defects persisted. Late treatment retinas exhibited continued, albeit slowed, loss of sensitivity and signal fidelity among RGCs, as well as persistent gliosis. We conclude that gene replacement therapies delivered after 50% rod loss are unlikely to restore visual function to normal. This is critical information for administering gene therapies to rescue vision.

## *Introduction*

Current gene therapies for photoreceptor degeneration can slow disease progression, but thus far, nothing fully stops cell death in preclinical models or patients[1,2]. One potential reason is that gene therapy involves several challenging technical confounds including viral design, mode of delivery, appropriate expression of the transgene, and stochasticity in cellular infection, all of which can produce abnormal levels of the therapeutic gene and/or limit the population of treated cells. By optimizing these parameters, it is possible to achieve complete gene delivery in surviving cells and normal levels of gene expression, which could fully stop photoreceptor death and restore normal vision. Alternatively, it is possible that once some amount of photoreceptor death occurs, gene therapy has a limited effect on halting additional cell loss, or on rescuing visual function.

To examine this issue, we used a mouse model of gene therapy for retinitis pigmentosa (RP) in which complete genetic rescue across the retina can be achieved without the use of viral vectors. This mouse does not express the beta subunit of the rod-photoreceptor cGMP-gated (CNG) channel because a neomycin cassette flanked by loxP sites was inserted into intron 19 of the *Cngb1* locus (*Cngb1*$^{neo/neo}$)[3–5]. This prevents CNGB1 expression and reduces the formation of CNG channels, ultimately leading to rod degeneration and death similar to humans with RP[6]. All rods are lost by ~6 months postnatal; cones begin to die at 3-4 months and are all lost by ~8 months[4,7]. To mimic gene therapy, we crossed this *Cngb1*$^{neo/neo}$ line with the *UBC-cre-Ert* line containing tamoxifen inducible cre recombinase[8]. By delivering tamoxifen, activated cre removes the neomycin insert to enable endogenous CNGB1 expression across all rods, thereby producing a best-case scenario for gene therapy[9] .

We used this model to determine the extent to which photoreceptor survival and retinal signaling depended on the level of rod death prior to rescuing CNGB1 expression. We induced genetic rescue at multiple ages corresponding to different amounts of rod and cone photoreceptor loss in animals of both sexes. First, we assayed retinal structure across 3 treatment timepoints and 4 post-treatment timepoints (12 cohorts), as well as controls from age-matched untreated or heterozygous littermates (48 mice total).

We treated mice at 1, 2, and 3 months of age corresponding to 25%, 50% and 70% rod loss, and 0%, 0% and 5% cone loss, respectively. Following treatment, we measured the amount of additional photoreceptor loss and the presence of retinal inflammation. We also measured changes in the fidelity of retinal signaling and receptive field structure of retinal 'output neurons', the retinal ganglion cells (RGCs), using a large-scale multi-electrode array. Importantly, the structural data and physiology data were collected from the same retinas, allowing a comparison between structural and functional recovery following treatment.

Following each treatment timepoint there was some persistent, but modest photoreceptor loss several months after treatment. However, late treatment exhibited persistent gliosis, indicative of inflammation, while this was not observed following early and mid treatment. Functionally, there was a striking difference between the early (1M) and mid (2M) treatments versus late (3M) treatment in terms of RGC function at cone-mediated light levels. The gain and fidelity of RGC signals recovered to levels nearly indistinguishable from wild-type (WT) following early and mid treatments, but they failed to recover following late treatment. Similar results were observed at rod mediated light levels, with early and mid treatment resulting in nearly normal RGC signaling while late treatment exhibited continued deterioration. These results indicate that even under best-case scenarios, gene therapies for photoreceptor degeneration ought to be delivered prior to ~70% rod loss for long-term vision restoration and that gene therapy for RP may not perform well under conditions with more than 50% rod loss. Thus, the timing of genetic rescue is a critical variable for restoring vision.

## *Results*

### Genetic rescue slows, but does not immediately stop photoreceptor death

To assess the extent to which the timing of therapy impacts rod photoreceptor rescue, we induced genetic rescue at three timepoints using tamoxifen chow. Early treatment was performed in mice 1 month

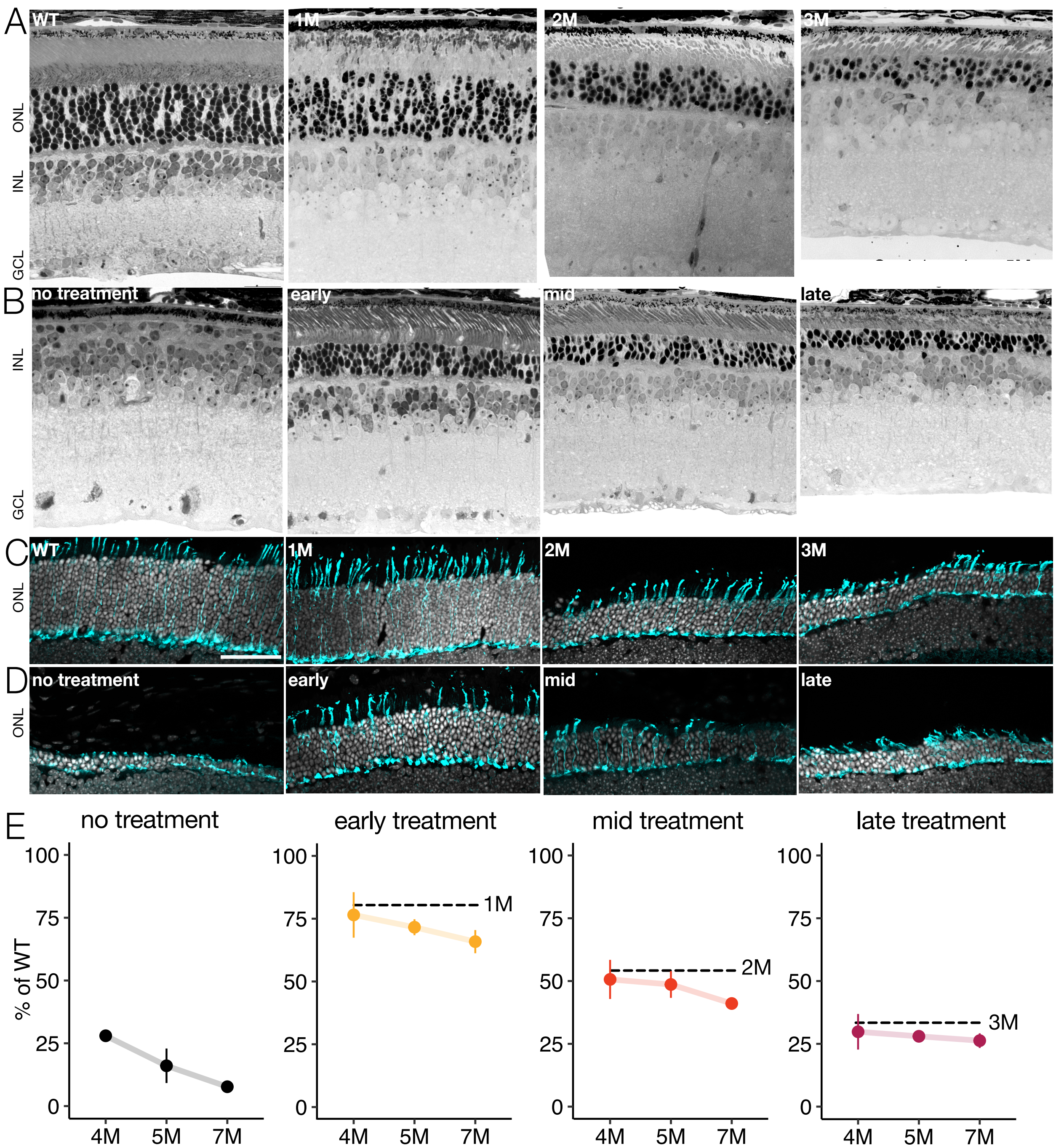


***Figure 1. Photoreceptor degeneration continues despite genetic rescue.** A) Light microscope images of retinal cross-sections from wild-type (WT) and* Cngb1$^{neo/neo}$ *mice at each treatment timepoint. Scale bar: 20 µm. B) Cross-sections from an untreated (*Cngb1$^{neo/neo}$;cre-*) retina (left) at 5M and three treated retinas after early, mid, or late treatment, each at 5M. C) Confocal images of retinal cryosections from WT and* Cngb1$^{neo/neo}$ *mice at each treatment timepoint. Cone structure in cyan (mCar) and nuclei in white (DAPI). Scale bar: 50 µm. D) Cross-sections from an untreated (*Cngb1$^{neo/neo}$;cre-*) retina (left) at 7M and three treated retinas after early, mid, or late treatment, each at 7M. E) Quantification of outer nuclear layer (ONL) cell counts over time to measure fraction of surviving photoreceptors. Dashed line indicates ONL thickness at time of treatment. Error bars indicate +/- 1 standard deviation. Measurements are from 5074 nuclei across 210 sampled regions (each region 1000 µm$^2$).*

(1M) of age with approximately 25% rod loss (Figure 1A) and no cone loss (Figure 1C). The mid treatment consisted of 2M mice with ~50% rod loss and no cone loss, and the late treatment was performed in 3M mice with ~70% rod loss and ~5% cone loss (Figure 1A, C) (prior quantification of cone loss provided in Scalabrino et al., 2022). Treated mice were sacrificed at 1-month intervals between ages 4M and 7M to measure the visual response properties of RGCs and to histologically assess the time-dependent effects of treatment on photoreceptor survival. We have shown that 7-day tamoxifen treatment produces robust cre-mediated recombination across surviving rods[9] and treatment restored CNGA1 expression, indicating genetic rescue resulted in intact channel formation (Figure S1). At all timepoints, tamoxifen treatment reduced rod and cone loss compared to untreated animals (Figure 1), with greater preservation in dorsal retina (Figure S2). However, there was a weak trend showing continued photoreceptor loss several months following treatment, as measured by the number of nuclei in the outer nuclear layer (Figure 1E). With early treatment, 76% of photoreceptors remain at 4M, but this dropped to 65% by 7M (p-value: 0.007, 1624 counted nuclei and 48 sampled regions). Next, with mid treatment, 51% of photoreceptors remain at 4M and decreased to 41% by 7M (p-value: 0.032, 1164 counted nuclei and 48 sampled regions). Finally, with late treatment, 30% of photoreceptors remain at 4M and decreased to 26% at 7M (p-value: 0.106, 739 counted nuclei and 51 sampled regions). These results suggest photoreceptor health is not fully stabilized following a treatment that cures the initial cause of rod death, though degeneration is substantially slowed. Surprisingly, the initial rate of continued cell death may be fastest with the earlier treatment (Figure 1E, 'early'). Despite these lower numbers of photoreceptors following treatment, outer segments of remaining rods (Figure 1B) and cones (Figure 1D) persisted.

**Synaptic structure is disorganized in late therapy**

Rod death causes many secondary changes including retinal rewiring, particularly in the outer plexiform layer[10–13]. Thus, we assessed how the structure of synaptic terminals depended on the treatment timepoint. Early treatment largely preserved rod and cone terminals, as assessed by staining for CtBP2, which is the major structural component of the synaptic ribbon between photoreceptors and bipolar cells (Figure 2A-B). CtBP2 labeling indicated normal 'horseshoe-like' synaptic structures were prevalent in retinas receiving the early treatment[14,15]. For mid-treatment, CtBP2 labeling continued to reveal horseshoe structures. Following late treatment, CtBP2 horseshoe structures were substantially reduced despite ~25% of rods and ~90-95% of cones remaining at this treatment timepoint. The sparser synapses following late treatment suggest that earlier treatment may be important for rescuing normal and long-lasting retinal function.

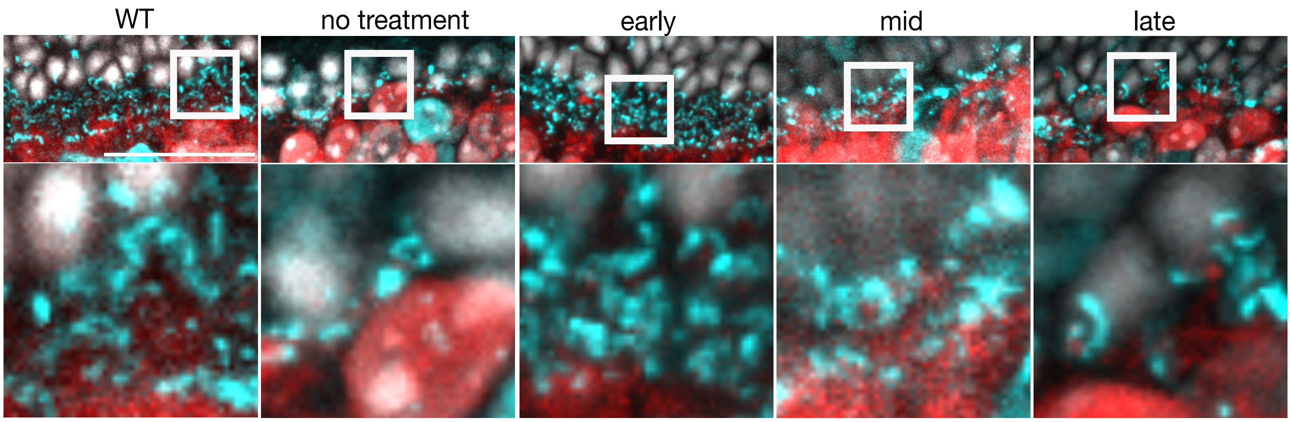


***Figure 2. Photoreceptor synapses are reduced but stable following treatment.*** *Histology of rod and cone synapses in cyan (CtBP2) at 7M from (from left to right) WT, untreated (*Cngb1$^{neo/neo}$;cre-*), early, mid and late treatment timepoints. Nuclei in white (DAPI) and rod ON bipolar cells in red (PCP2) to visualize approximate location of bipolar cell bodies and dendrites. Square region in top row enlarged below. Scale bar: 50 µm.*

**Gliosis present in late treated retinas**

As a final measure of retinal structure following time-dependent rescue of *Cngb1*, we investigated the activation of Müller glia by immunolabeling glial fibrillary acid protein (GFAP)[16]. This marker indicates a retinal inflammatory response, which is present in patients with RP[17–19]. While this response can protect the retina from damage (e.g., by releasing neuroprotective molecules)[20,21], prolonged activation can increase tissue damage through the release of pro-inflammatory markers[22]. We found GFAP labeling was minimally present in early or mid treatment retinas examined at 7M. However, we found that GFAP was present in both untreated and late treated retinas at 7M (Figure 3). This indicates a prolonged retinal stress response and pathology despite genetic rescue: GFAP labeling was present 4 months after the

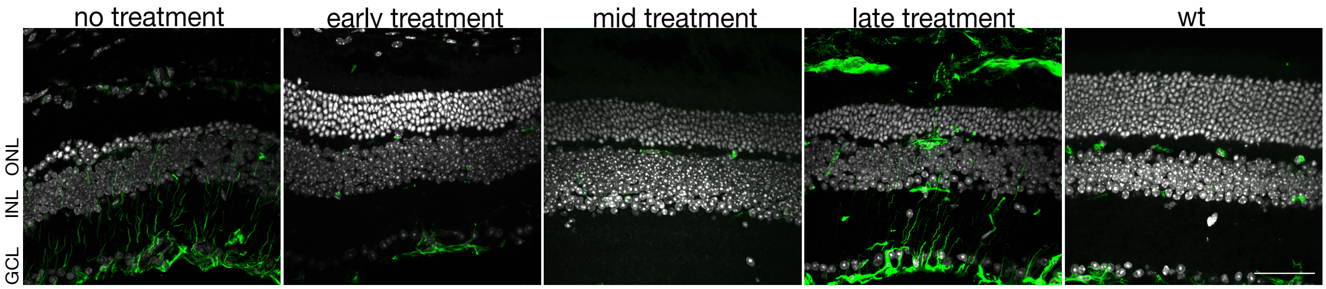


***Figure 3. Activated glia present in late treated retina.*** *Immunofluorescence shows GFAP (green) expression in 7M retinas (left to right): WT, untreated (cre-), early, mid and late treatment time points. Nuclei labeling with DAPI shown in white. Scale bar: 50 µm. ONL = outer nuclear layer; INL = inner nuclear layer; GCL = ganglion cell layer.*

late treatment timepoint. Importantly, this is independent of viral gene therapy, which is also known to invoke an immune response. Thus, late treatment did not markedly improve glia-induced retinal inflammation.

**Late genetic rescue fails to restore gain of RGC responses at cone-mediated light levels.**

The preceding histological assessments suggest that retinal function might be compromised with late treatment relative to the early and mid treatment timepoints. However, previous studies have also indicated that retinal function can remain relatively robust despite marked changes in photoreceptor morphology and density in the *Cngb1*$^{neo/neo}$ and *rd10* models of RP[4,5]. To determine the impact of treatment timepoint on retinal function, we measured visual responses among RGCs, the output neurons of the retina, using a large-scale multielectrode array (MEA)[23–25]. In total, we measured responses from 22,783 RGCs. We focused on RGCs because changes in their response properties capture the net effects of degeneration and treatment on the signals transmitted from the retina to other brain areas[4]. We began by comparing receptive field properties of RGCs following the early, mid, and late treatment timepoints. Receptive fields summarize the spatial and temporal integration performed by RGCs and their presynaptic circuits as well as summarize the visual features that are signaled by RGCs to the brain[26,27]. We measured receptive fields at a photopic (cone-mediated) light level (10,000 Rh*/rod/s). We also focused on measuring the impact of rod *Cngb1* rescue on cone-mediated vision because we have shown previously that *Cngb1* rescue restores normal rod signaling[9]. Furthermore, the impact on cone-mediated vision is likely to be most informative and impactful for human-directed gene therapies.

To measure the receptive fields of RGCs, we presented checkerboard noise stimuli while recording RGC spikes with a large-scale MEA. In a typical experiment, we measured the responses of 250-430 RGCs simultaneously. Spatiotemporal receptive fields were estimated by computing the spike-triggered average to the checkerboard stimulus[26]. This provides an estimate of the linear component of the spatiotemporal receptive field. To analyze separately the changes in spatial and temporal receptive fields, we focused our analysis on RGCs with space-time separable spike triggered averages (see

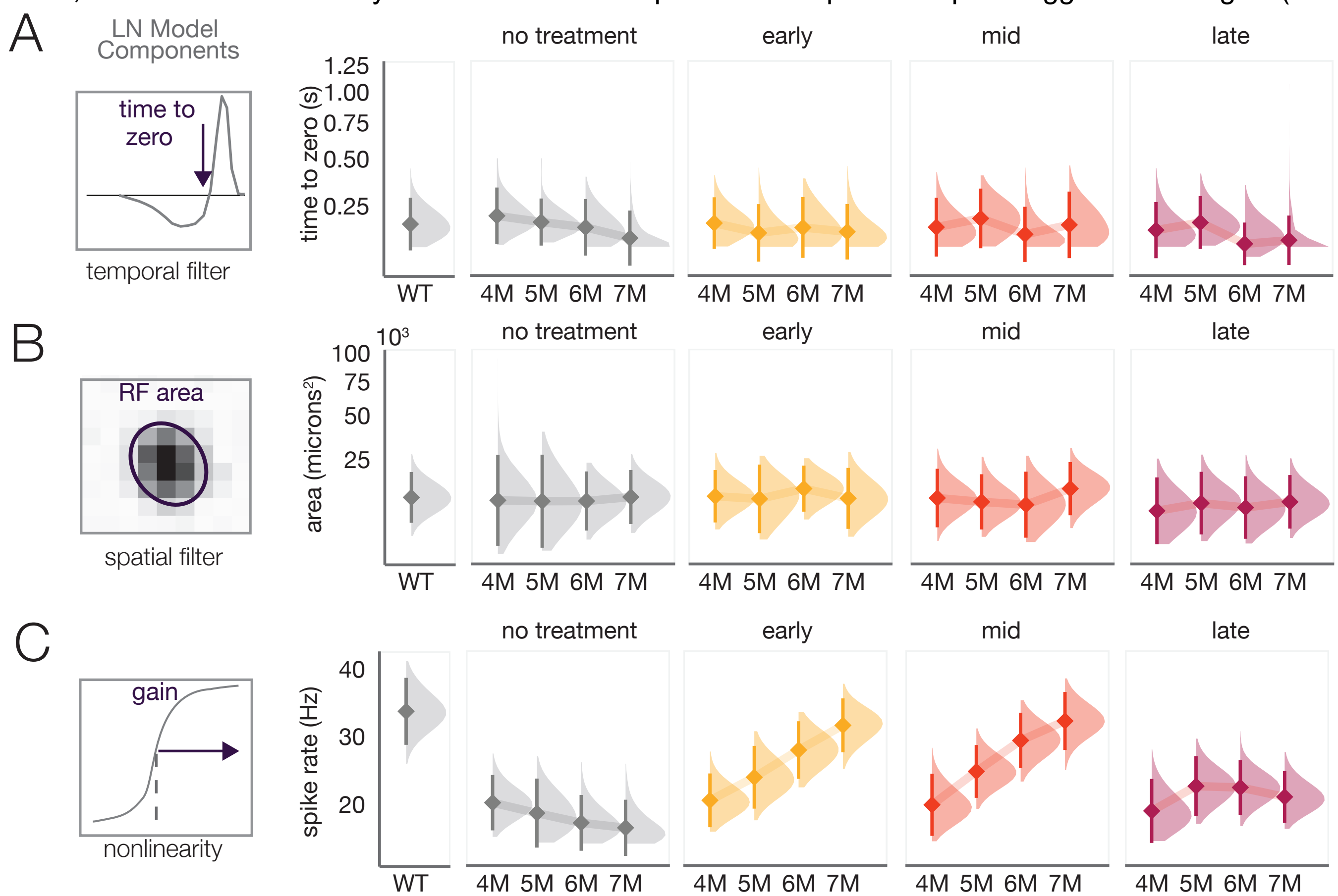


***Figure 4. Receptive fields are stable following treatment, but response gain is not recovered following late treatment**. A) Left: example temporal receptive field (RF) of an RGC, showing how the stimulus (on average) changed immediately preceding a spike. Arrow indicates time-to-zero used to estimate the integration time. Right: panels show distributions of the time to zero (diamond is the mean and bar is +/- 2 SD) in WT, no treatment, early, mid and late treatment retinas from 4-7M. B) Left: Spatial RF of an example RGC, ellipse is the 2-sigma contour of a 2-dimensional Gaussian fit. The geometric mean of the major and minor axes of the ellipse was used to estimate RF area, right: same as A-right but for RF size. C) Left: example contrast response function. Spike rate at 50% of peak was used to estimate gain. Right: same a A-right but for gain estimates. Light level 10,000 Rh*/rod/s.*

Methods)[4]. Variability in receptive field measurements may arise from variability in experimental preparations, sex of animals, and neuronal cell type. As such, a mixed effects model was used to determine associations between treatment time point and RGC physiology to account for potential confounds (see Methods). Changes in photopic temporal receptive fields were subtle in all treated retinas, largely because the temporal receptive fields changed little between 4 and 7M in untreated animals under photopic conditions (for example, at early rescue 3% difference in mean was observed between 4 and 7M; p-value: 0.34) (Figure 4A)[4]. The biggest change was in the late treatment group where receptive fields appeared to slow relative to WT at the 5M time point, but even this change was small and was not statistically significant (6.7% and 7%, respectively; p-values: 0.13, 0.11) (Figure 4A). Thus, the duration of temporal integration within RGC receptive fields was relatively stable following genetic rescue and did not depend on the treatment time point between 1M-3M (25-70% rod loss).

We also analyzed the size of spatial receptive field centers across RGCs. Like the temporal receptive fields, spatial receptive fields from treated animals were similar in size to WT and did not decrease over time (for example, at early rescue, 2% difference in mean was observed between 4 and 7M; p-value: 0.34) (Figure 4B); this is likely because there were minimal changes to the spatial receptive fields of untreated animals at even at 7M under photopic conditions (Figure 4B, gray distributions). These results indicate that spatial and temporal receptive field structure between 4-7M post-treatment do not depend strongly on the treatment time point. This is not particularly surprising because cone-mediated receptive field structure is relatively robust even to severe rod loss and changes in cone morphology[4,5].

We next examined the contrast response functions of the RGCs. Also referred to as 'static-nonlinearities' in reverse correlation analyses[26], the contrast response functions capture how many spikes an RGC tends to produce for a given similarity (correlation) between the stimulus and the receptive field. In untreated retinas, there was a diminished gain between 4-7M relative to WT retinas (Figure 4C, gray distributions). Thus, genetic rescue had the potential to improve response gain and transform visual responses to be more similar with WT. Indeed, early treatment improved gain to near WT levels by 7M (14% difference; p-value: 0.11) (Figure 4C). Mid treatment also improved gain to near WT levels at 7M

(15% difference; p-value: 0.15). Interestingly, for both early and mid treatment, gain rose over several months following treatment, suggesting this increase resulted from both changes in photoreceptor health and retinal wiring (see Discussion).

Unlike early and mid treatment, late treatment produced a modest recovery of gain that was higher than untreated animals at 7M (at 7M, 20% higher relative to 4M; p-value: 0.01), but substantially lower than animals treated at 1M or 2M (Figure 4C). Qualitatively similar results were obtained at a mesopic light level (100 Rh*/rod/s) (Figure S3). Thus, this late treatment timepoint was ineffective at restoring the contrast response gain at cone-mediated light levels despite 25% of the rods and 95% of the cones remaining at the time of treatment[4].

**Late genetic rescue results in higher noise.**

Above we showed that late treatment results in reduced response gain across the RGC population. We wondered if there was also a change in RGC response variability, or ‘noise’. This is important because greater noise in the response will result in less reliable signaling of visual information. There are two potential sources of increased noise: signal-independent and signal-dependent. Signal-independent noise manifests as increased spontaneous activity in RP[28–30]. However, we previously found that *Cngb1*$^{neo/neo}$ mice do not exhibit increases in spontaneous activity or spontaneous oscillations until nearly all the photoreceptors have died (8-9M in untreated animals)[4], indicating there is not an increase in signal-independent noise.

To examine signal-dependent noise, we measured the variance in the spike count while presenting a repeated checkerboard stimulus (Figure 5A). Higher variance in the spike counts to a repeated stimulus indicates an increase in signal-dependent noise given no change in signal-independent noise. For a Poisson process, the variance in spike rate is approximately equal to the mean spike rate (Figure 5B-C, solid line). WT responses fell along this line (black dots, Figure 5B-D), indicating they were

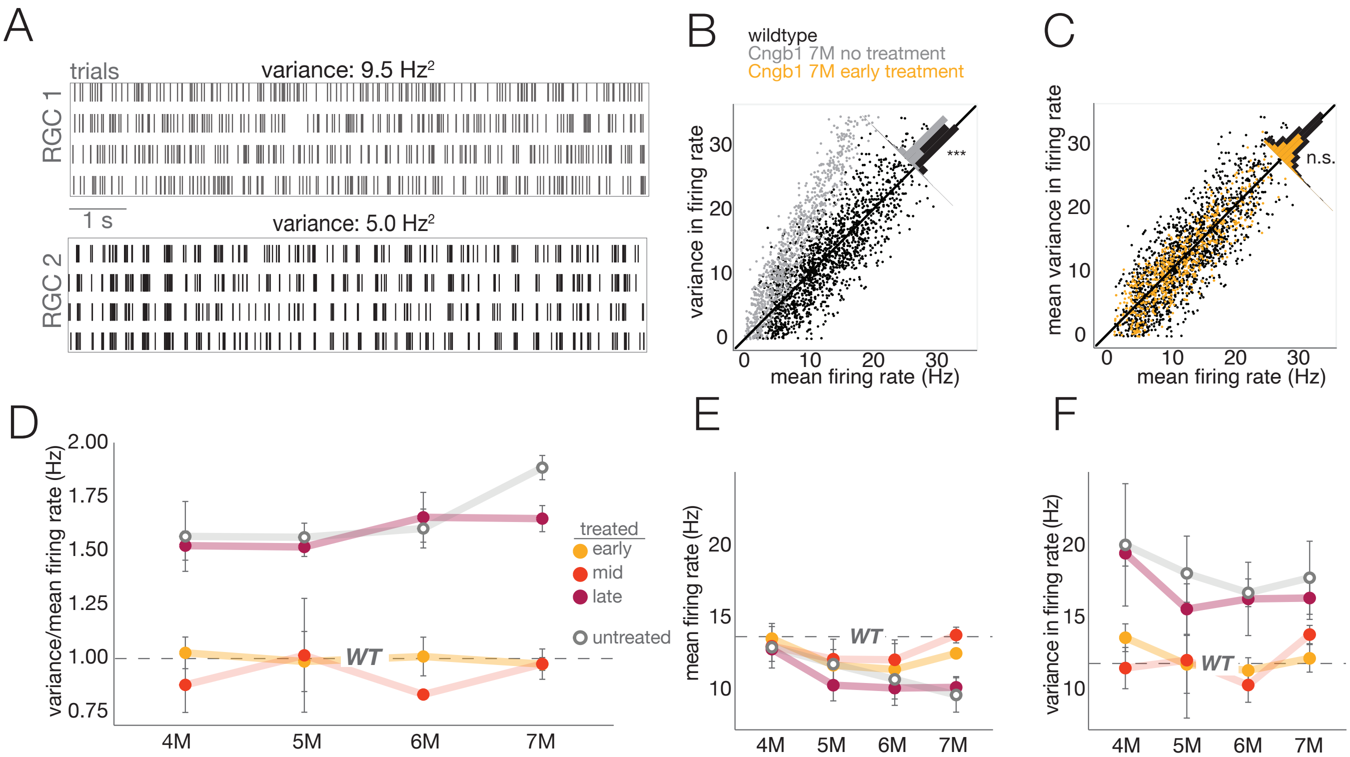


***Figure 5. Signal variance remains high following late treatment****. A) Two example RGC responses to photopic checkerboard noise repeats with similar firing rates but different temporal variability in firing rates. B) Variance and mean firing rates of RGCs in WT (black) and 7M untreated (gray) RGCs (temporal bin size was 5 ms). C) Same as B, comparing WT (black) and early treated (yellow) RGCs, measured at 7M post treatment. D) Average variance/mean firing rate ratio +/-2 SD after treatment for different treatment timepoints. Dashed line shows WT value, which did not depend on age over the range of sampled timepoints. E) Mean firing rate and F) mean observed variance in firing rate +/-2 SD after treatment for different treatment timepoints.*

approximately consistent with a Poisson process when using a checkerboard noise stimulus. However, responses from *Cngb1*$^{neo/neo}$ mice exhibited a clear tendency to lie above this line, indicating higher variance responses for a given mean (Figure 5B, D). Early and mid treatment brought the response variability back toward that of WT. However, late treatment failed to reduce the signal-dependent noise, which lingered near that of untreated *Cngb1*$^{neo/neo}$ RGCs even at 7 months post treatment (Figure 5C-D, F). These results indicate that the treatment time point is critical for robustly and stably reducing variability in cone-mediated RGC responses.

**Late treatment fails to rescue visual information.**

Thus far we have shown that late treatment at 3M (70% rod loss) fails to restore the gain of RGC responses to WT or near WT levels (Figure 4C) and results in increased response variability to a checkerboard stimulus (Figure 5D). Decreased gain and increased variability should result in less information transmission from the retina to the brain. To assess directly the information content of RGC responses, we presented a repeated 10s checkerboard stimulus (see Methods) and calculated the mutual information between RGC responses and the stimulus[4,31]. Mutual information indicates how much observing an RGC response reduces uncertainty about the stimulus[32]. RGCs with highly reproducible responses will generally provide more information about a stimulus (Figure 6A, RGC 1) than those with less reproducible responses (Figure 6A, RGC 2). In treated retinas, the cone-mediated information rate from early and mid treatment retinas increased by 5% and 9.5%, respectively, relative to untreated retinas shortly after therapy (4M and 5M; p-values: 0.04, 0.01), and approached WT levels by 6M (Figure 6B). However, in the late treated retinas, information declined over time (20% decrease in cone-mediated information transmission at 7M relative 4M; p-value: <0.001) (Figure 6B). In sum, late treatment resulted in information rates that were substantially greater than untreated animals, but also far less than earlier treated and WT animals. These results further indicate that late treatment of rod degeneration does not ultimately restore normal cone-mediated signaling among RGCs.

We have shown previously that rescuing CNGB1 expression in rods restores rod light responses and dim-flash sensitivity among RGCs[9]. However, we did not show how rod rescue impacts RGC information rates at rod-mediated light levels. We were curious if there are similar differences in early, mid and late treatment timepoints among RGCs under scotopic conditions as we have observed for photopic conditions. At a mean light level of 1 Rh*/rod/s, we presented a repeating checkerboard stimulus and calculated the mutual information between the stimulus and the RGC responses. In untreated animals, the rod-mediated information rate was undetectable due to the lack of CNG-channels, which results in diminished photocurrent that leads to hyperpolarized rods[9]. However, early treatment restored rod-mediated signaling to WT levels by 7M (3% lower than WT; p-value: 0.82) (Figure 6C). Interestingly,

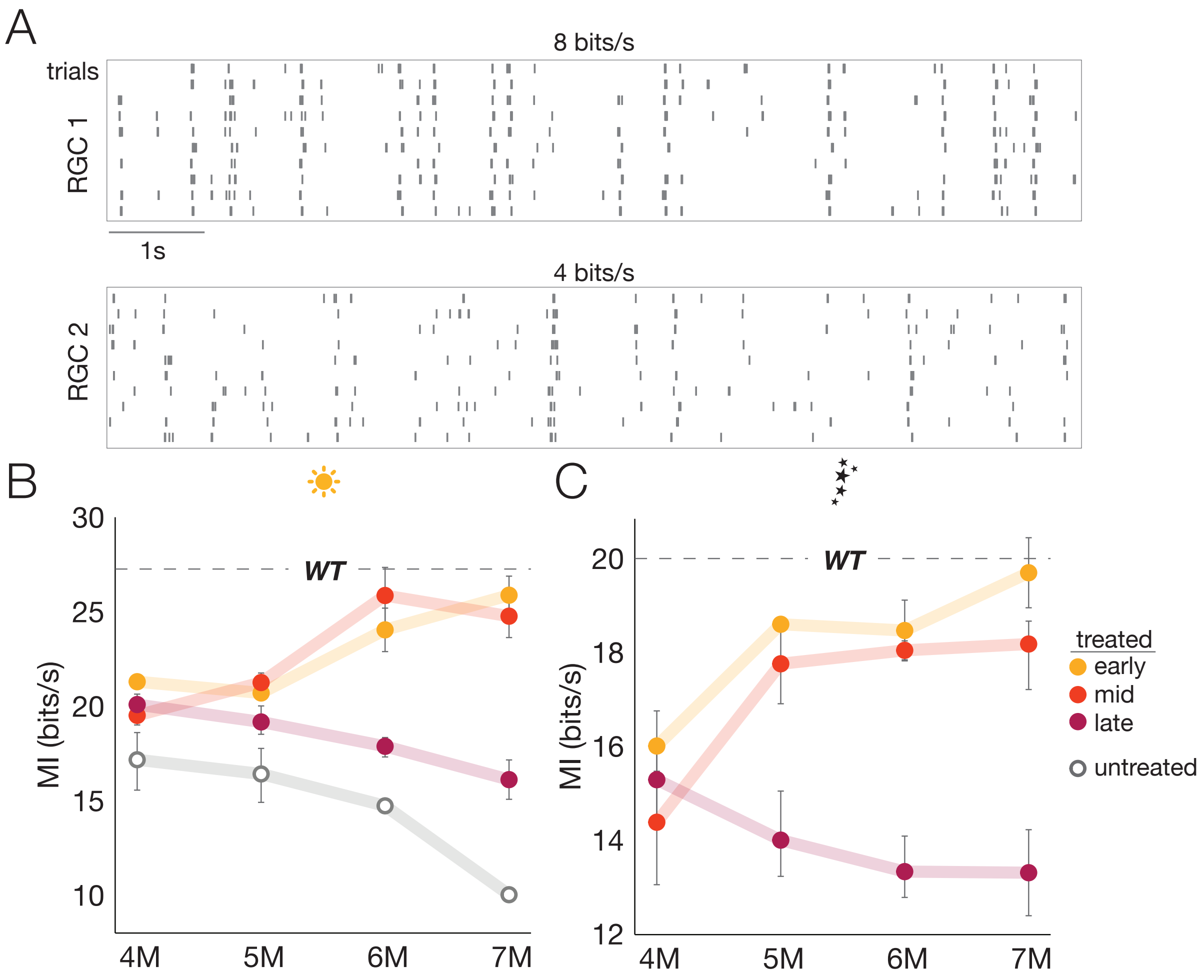


***Figure 6. Information transmission is not recovered following late treatment*** *A) Two example RGC responses to photopic white noise repeats near the median information rate (top) and near the 25th percentile (bottom) in an experiment. Mean +/- 2 SD mutual information rate of RGC responses (n = 2-6 retinas) at B) photopic and C) scotopic light level from the top 10% most informative RGCs. Dashed line indicates the mean information rate observed in RGC responses from WT retinas.*

the information rate at 4M for early treatment was only 22.8 bits/sec (17% lower than WT; p-value: 0.02), indicating it requires several months for information rates under scotopic conditions to reach normal levels following *Cngb1* rescue. Similarly, mid treatment also improved rod information transmission over several months, but the information rates did not quite recover to WT rates by 7M (5 months post-treatment). Late treatment also improved the information rate of the rod-mediated RGC signaling above baseline (which was essentially 0 bits/s in untreated animals), but the information rate declined over the months following treatment (Figure 6C; 15% lower at 7M than 4M; p-value: 0.03), and never achieved information rates near those of WT RGCs (32% less than WT at 7M; p-value: 0.0001). Thus, late treatment was not sufficient to fully restore rod-mediated retinal signaling and signaling declined in the months following treatment. These results were also consistent for visual responses recorded at a mesopic light level (Figure S4). To ensure these results were not specific to a checkerboard stimulus, we also presented a repeated natural movie and obtained similar results under scotopic conditions (Figure S5).

## Discussion

In the coming years, significant resources will be devoted to the development of therapies for rare diseases, including those caused by *CNGB1* mutations (*CNGB1*-RP, a.k.a. RP45), which was recently highlighted as a key gene therapy target by the NIH supported Accelerating Medicines Partnership Bespoke Gene Therapy Consortium. Defining gene therapy intervention points is essential to developing effective treatments that both restore and maintain vision. In this study, we addressed the question of how a preclinical mouse model for RP responds to a therapeutic intervention. We show that early (25% rod loss) and mid (50% rod loss) treatment did not completely halt photoreceptor loss. However, early and mid treatment timepoints did restore rod- and cone-mediated visual signaling among RGCs. Interestingly, this restoration took a few months to complete, suggesting that some rewiring and/or circuit stabilization were required after genetic rescue. Following late intervention (70% rod loss), retinas exhibited evidence for persistent inflammation gliosis and visual signaling among RGCs continued to steadily decrease under both rod- and cone-mediated conditions. These results indicate gene therapy interventions for CNGB1-RP may not succeed in preserving the remaining rod or cone vision if delivered after 50% rod loss.

### Comparison to other studies

Gene therapy is a growing field for a variety of photoreceptor degenerations, including RP (see review by Nuzbrokh et al., 2021). Several studies have assessed AAV-mediated gene replacement in both mouse and canine models of CNGB1-RP. Mouse studies found that regardless of intervention time or dose, *Cngb1* gene replacement improves function, but fails to halt cell death[34–36]. Additionally, AAV-*Cngb1* treatment was compared between rodent and canine models of CNGB1-RP[37]. In both species, early intervention was correlated with improved results, indicating this trend is not mouse specific. Considering these results from other studies, our findings indicate that insufficient vector dosage is not the primary factor impeding recovery; rather, gene replacement is not enough to fully correct pathology, particularly degeneration, once significant cell death has occurred.

Studies on additional models of RP have shown greater viability in gene therapy success following late-stage intervention. Using an inducible cre system to correct Pde6b-RP, two studies investigated the differences between full rescue at early, mid, and late stages of degeneration, and partial rescue at an early timepoint[38,39]. The full rescue study showed late intervention minimally improved scotopic photoreceptor and bipolar cell function (as measured by electroretinography, or ERG), but degeneration was halted at all timepoints[38]. The partial therapy failed to recover light responses at any dose and degeneration continued, though the authors attributed this to death of untreated cells[39]. The cause of the discrepancy between our study showing continued cell death and the 2015 study is unclear: differences could be caused by the mutation, intervention time, or rate of degeneration. It is also possible that disease state, such as increased inflammation, plays a significant role in the amount of cell death occurring, at least in photoreceptor loss from *Cngb1* mutations.

A technical difference between our study and previous work on genetic rescue for RP is the use of large-scale MEAs to measure the physiological impact of genetic rescue rather than ERGs. ERGs have the advantage that they can be performed *in vivo* and can thus track the responses of photoreceptors and bipolar cells over time and following treatment in individual animals. They have the disadvantage that they average the responses of many cells and thus provide minimal insight into noise or signal fidelity, and mostly reveal changes in gain and response kinetics but without identifying the cellular location or molecular mechanism. Furthermore, they assay outer-retinal function, but photoreceptor degeneration could also alter inner retinal function[11]. MEA measurements have the disadvantage that they are *ex vivo* and thus can only examine one timepoint per animal. However, MEA measurements have the potential advantages of providing more refined information about changes in receptive field structure, gain, noise, and information rates among individual and populations of RGCs, the output neurons of the retina. In the end, these methods are complementary approaches that could be used productively together to dissect the impact of photoreceptor degeneration and genetic rescue across multiple aspects of retinal physiology.

**Therapeutic targets**

People with RP are not typically diagnosed until after significant rod loss and the onset of cone dysfunction, particularly those with *CNGB1* mutations[40]. While the timeline of disease progression and diagnosis varies quite considerably, for CNGB1-RP median diagnosis occurs at 27 years, though most patients report nyctalopia at infancy/childhood and retain only central vision by their diagnosis. This timing is unfortunate based on the findings that early intervention results in better and more long-lasting visual function; by the time a patient is diagnosed, they are well past the early and mid intervention windows of 25-50% rod loss that we examined. However, while late treatment does not halt degeneration and does not improve visual responses to normal, the improvements may be enough to restore behaviorally useful vision, and that vision may last for the lifetime of the patient. Future studies should assess visual behaviors in late-treated animal models.

Our study and others point to several additional therapeutic targets that may be important for improving outcomes for RP patients. First is targeting cone photoreceptors. Given that foveal cones persist much longer than rods and peripheral cones, preserving cone vision is an attractive target for new therapies. It is unknown why cones eventually die in this disease, despite not needing the causative gene (*Cngb1*) to function. There are several potential sources of continued degeneration that could be targeted in addition to gene replacement: metabolic stress, lack of rod-derived trophic factors, inflammation, or lack of structural support[41–43]. Thus, therapies aimed at cones have the benefit of having a long intervention timeframe, maintaining the range of vision that is most used by humans, and being mutation-independent, thus applicable to a wide variety of photoreceptor degenerations.

A second therapeutic target relates to reducing inflammation[17]. Activated glia were present in the late treatment group of our study (Figure 3), indicating the retina remained stressed despite curing the underlying cause of degeneration. Viral gene therapy will only worsen inflammation. Anti-inflammatories or other neuroprotective molecules may alleviate this form of disease pathogenesis, allowing the retina more opportunity to heal.

A third therapeutic target is synaptogenesis in the outer plexiform layer. While the retina appears to compensate for reduced synapses[4], it does need a certain number of intact photoreceptor-bipolar cell connections to maintain information flow. We found treated retinas had reduced outer plexiform structure relative to wild-type retinas, presumably from bipolar cells losing their pre-synaptic partners. Increasing synaptogenesis is an attractive target to improve retinal signaling particularly for improving the outcomes of late treatment.

**Open questions**

We found that recovery of light responses took several months to recover following gene correction, rather than several weeks. It remains unclear what circuit level changes occur during this dynamic period after therapy. Future studies are needed to yield insights into the recovery process mechanisms, which could then be harnessed to extend the window of therapy to later time points.

An important next step for assaying the impact of diverse therapeutic approaches for treating RP and other retinal degenerative diseases is to develop better visually guided behavioral assays for rodents. Water mazes are low throughput and stressful on the animals, while the optokinetic reflex likely circumvents pathways for non-reflexive visual behaviors. Cricket hunting is one emerging behavior for use in rodents and primates that offers several attractive features[44,45]. The behavior requires almost no training and demands that the animal use visual input to execute coordinated and dynamic motor outputs. As such, it may offer greater sensitivity to subtle changes in vision than alternative approaches, while being relatively high throughput and easy for many labs to utilize.

Finally, we recognize artificial gene replacement in a mouse model of disease is not translational to human therapeutics. Rather, these results yield insights into the best a therapy could achieve if improvements are made on the gene delivery front such as better cell penetration or expression of therapeutic genes. It is essential to perform these studies in additional models with retinas and visual systems which are more similar to human retina and human vision.

## Methods

### Animal model

Mice were used in accordance with the Duke University Institutional Animal Care and Use Committee guidelines (protocol A084-21-04) and the Association for Research in Vision and Ophthalmology. *Cngb1$^{neo/neo}$* mice[3,9] were crossed with UBC-cre/ERT2[8] (JAX stock #007001, RRID: IMSR_JAX:007001) to generate mice with tamoxifen inducible genetic rescue of *Cngb1*. Mice were housed in a facility with a 12h light/dark cycle and fed chow ad libitum. Both sexes were used (21 female, 19 male). Wild-type and untreated *Cngb1$^{neo/neo}$* controls consisted of littermates; a portion of these animals were fed tamoxifen (only *Cngb1$^{neo/neo}$* that were cre-). All genotyping was performed by Transnetyx using primers for neomycin FWD GGGCGCCCGGTTCTT, REV CCTCGTCCTGCAGTTCATTCA, PROBE ACCTGTCCGGTGCCC and WT allele FWD TCCTTAGGCTCTGCTGGAAGA, REV CAGAGGATGAACAAGAGACAGGAA, PROBE CTGAGCTGGGTAATGTC.

### Treatment

Tamoxifen chow (Envigo, TD.130858, 0.5g/kg tamoxifen) replaced rodent chow (PicoLab 5053) for 7 days and was provided ad libitum. Efficacy of tamoxifen treatment leading to genetic rescue has been previously described[9]. Mice were monitored during treatment to ensure no adverse effects to the drug. Mice that showed signs of illness were switched back to non-tamoxifen rodent chow and removed from the study. Additionally, select mice were confirmed to have recombined *Cngb1* using Transnetyx.

### Histology, microscopy, and quantification

Histology was performed as previously described[4,9]. Antibodies used included mCar (1:500, Millipore AB15282, RRID: 652 AB_1163387), PCP2 (1:500, Santa Cruz sc-137064, RRID: AB_2158439), CtBP2

(1:1000, BD Biosciences Cat# 612044, RRID:AB_399431), GFAP (1:400, Sigma-Aldrich Cat# G3893, RRID:AB_477010), CNGA1 (1:50, generously provided by R. Molday[46]), Alexa Fluor donkey anti mouse 647 (1:500, Thermo Fisher Scientific Cat# A-31571, RRID:AB_162542), and Alexa Fluor donkey anti rabbit 555 (Thermo Fisher Scientific Cat# A-31572, RRID:AB_162543).

All images were taken from dorsal retina unless otherwise noted. Light microscope images were captured with a Zeiss Axioplan2 microscope using a 63x air objective. Confocal images were taken using a Nikon AR1 confocal microscope using a 60x oil objective and motorized stage. Images were processed using FIJI software[47].

Photoreceptor quantification was performed across 3 steps, which included preprocessing, automated quantification, and then manual count corrections. Images were processed to include 15 z-slices (0.5 μm each) of the outer nuclear layer. Image contrast was then adjusted to maximize local contrast using the Integral Image Filters plugin at default parameters. Next, we used a custom Matlab script to detect nuclei in the preprocessed images. For each image, we sampled 3 rectangular regions (1000 square microns) that were located approximately center, left, and right within the ONL. These three counts were averaged for each retina. Images were converted to a binary map to detect high intensity areas using a threshold of 0.4 or a pixel value of 104 for 8-bit images. These high intensity areas were restricted to those that had a minimum width of 2.1 μm and were located at least 1.05 μm away from its neighbors. Due to these parameters, approximately 5-10% of visible nuclei or about 5-15 nuclei in each sampled region were out of focus and were not automatically counted. Thus, in the final step, nuclei which were missed were manually counted.

**MEA recordings**

All recordings were performed as described previously{Citation}. Briefly, mice were dark adapted overnight by placing their home cage with food and water into a light shielded box fitted with an air pump. All procedures were performed under IR illumination using night vision goggles. Following decapitation, eyes were enucleated and placed in bubbled room temperature Ames media (Sigma, A1420) for the duration of the dissection. Eyes were then hemisected, vitrectomy performed, and retina detached from RPE and sclera. A ~1x2 mm dorsal retinal piece was cut and placed RGC side down on a 519 dense multielectrode array with 30 μm spacing[24,48,49]. Throughout the recording, 32°C bubbled Ames was refreshed at a rate of ~6mL/min.

**Spike sorting and neuron identification**

Spikes for each of the electrodes were identified by using 4 times the voltage standard deviation[50,51]. Spike sorting was performed by an automated PCA algorithm described previously[25]. To track identified RGCs across light conditions and stimuli, cell clusters were sorted in the same PCA subspace at each light level. Neurons were verified as matches across stimulus and light conditions by examining their spike waveforms and electrical images[25]. RGCs were classified at the photopic light level by clustering cells according to their receptive field properties and spike-train autocorrelation functions.

**Visual stimuli**

Visual stimuli were described previously[4]. Visual stimuli consisted of binary checkerboard noise and natural movies[52,53], presented using a gamma-calibrated OLED display (Emagin, SVGA + XL Rev3) focused by a 4x objective (Nikon, CFI Super Fluor ×4) attached to an inverted microscope (Nikon, Ti-E). For scotopic (~1 Rh*/rod/s) and mesopic (~100 Rh*/rod/s) checkerboard stimuli, each square was ~150x150 μm and refreshed every 66 ms. Photopic (~10,000 Rh*/rod/s) checkerboard squares were each 75x75 μm and refreshed every 33 ms. Repeat movies consisted of a 10s clip of either checkerboard or natural movies repeated 100x. Checkerboard repeats had the same parameters at a given light level as described above.

**Spike triggered averaging and nonlinearity calculations**

Spike triggered averaging (STA) was used to estimate the linear component of the receptive fields for each RGC. Procedures for calculating the spatiotemporal receptive field were identical to those described previously[4]. We analyzed the spatial and temporal receptive fields of RGCs for which at least 60% of the variance in the STA was captured by a rank-one factorization. Cells which had a temporal filter that were biphasic were included because a well-defined zero crossing time was necessary for estimating the time to zero. 85% of space-time separable STAs met this criterion. Static nonlinearities were calculated for RGCs with space-time separable STAs by mapping the convolution of the linear filter and checkerboard stimulus with their response[26]. These static nonlinearities were used to characterize the contrast-response function of individual RGCs and their response gain.

**Mutual information**

Shannon's definition of entropy was used to measure mutual information with the use of the 'direct method' described previously[4,54]. Spike trains were binned according to entropy estimates that achieved the Ma Upper Bound[55] and ranged from bins of 4-6 ms and formed patterns of 3-6 bins. Mutual information was thus computed as:

$I(S;R) = H(R) - H(R;S)$

where $H(R)$ is the entropy in the response and $H(R;S)$ is the entropy of the response conditioned on the stimulus.

**Statistical analysis**

Kolmogrov-Smirnov tests were used to determine differences between treatment groups. P-values were corrected for multiple comparisons by Bonferroni correction. To measure whether differences across timepoints could be produced by other factors (e.g., experiment-to-experiment variability), a parametric linear mixed effects model was used . The mixed effects model accounts for retina-to-retina variability by adding each experiment as a random effect. This procedure permitted making broad-level inferences about the RGC populations without dependence on experimental variability. In addition, the sex of the animal and a neuron's cell type was considered by including them as interaction terms with the treatment conditions. This step enabled determining whether treatment conditions were associated with information rates and receptive field sizes in a sex-independent fashion. The model indicated that conclusions about the impact of genetic rescue on RGC signaling were insensitive to sex, experimental variability, and cell type.

**Data Availability**

Source data and code used to generate figures are available in the github repository https://github.com/mishek-thapa/treatment_paper. Raw data and the *Cngb1*$^{neo/neo}$ mouse model are available upon request by contacting the corresponding author. Raw images for Figures 1-3 can be found at https://doi.org/10.5061/dryad.rv15dv4bv.

**Author contributions**

Experimental design: MS, JC, AS, GF

Histology experiments: MS, TW

MEA experiments: MS

Histology analysis: MS, MT, JC

MEA analysis: MS, MT, GF

Writing: MS, MT, GF

Editing: MS, MT, GF

**Acknowledgements:**

We thank our funding sources: National Institute of Health (NIH) R01 EY027193 (GDF, APS, and JC), NIH NEI core grant EY5722, Holland Trice Foundation, Whitehead Foundation, and Research to Prevent Blindness unrestricted grant to Duke University. We thank Dr. S Roy for helpful discussions on information theory.

## *References*

1. Cheng, S. Y. & Punzo, C. Update on Viral Gene Therapy Clinical Trials for Retinal Diseases. *Hum. Gene Ther.* **33**, 865–878 (2022).
2. Wang, X., Yu, C., Tzekov, R. T., Zhu, Y. & Li, W. The effect of human gene therapy for RPE65-associated Leber's congenital amaurosis on visual function: a systematic review and meta-analysis. *Orphanet J. Rare Dis.* **15**, (2020).
3. Chen, J. *et al.* Channel modulation and the mechanism of light adaptation in mouse rods. *J. Neurosci. Off. J. Soc. Neurosci.* **30**, 16232–40 (2010).
4. Scalabrino, M. L. *et al.* Robust cone-mediated signaling persists late into rod photoreceptor degeneration. *eLife* **11**, (2022).
5. Ellis, E. M. *et al.* Cones and cone pathways remain functional in advanced retinal degeneration. *Curr. Biol.* (2023) doi:10.1016/j.cub.2023.03.007.
6. Dryja, T. P. *et al.* Mutations in the gene encoding the alpha subunit of the rod cGMP-gated channel in autosomal recessive retinitis pigmentosa. *Proc. Natl. Acad. Sci. U. S. A.* **92**, 10177–10181 (1995).
7. Hüttl, S. *et al.* Impaired Channel Targeting and Retinal Degeneration in Mice Lacking the Cyclic Nucleotide-Gated Channel Subunit CNGB1. *J. Neurosci.* **21**, 130–138 (2005).
8. Ruzankina, Y. *et al.* Deletion of the developmentally essential gene ATR in adult mice leads to age-related phenotypes and stem cell loss. *Cell Stem Cell* **1**, 113–126 (2007).
9. Wang, T. *et al.* Activation of Rod Input in a Model of Retinal Degeneration Reverses Retinal Remodeling and Induces Formation of Functional Synapses and Recovery of Visual Signaling in the Adult Retina. *J. Neurosci.* **39**, 6798 LP – 6810 (2019).
10. D'Orazi, F. D., Suzuki, S. C. & Wong, R. O. Neuronal remodeling in retinal circuit assembly, disassembly, and reassembly. *Trends Neurosci.* **37**, 594–603 (2014).
11. Jones, B. W. *et al.* Retinal remodeling triggered by photoreceptor degenerations. *J. Comp. Neurol.* **464**, 1–16 (2003).

12. Lee, J. Y., Care, R. A., Santina, L. D. & Dunn, F. A. Impact of Photoreceptor Loss on Retinal Circuitry. *Annu. Rev. Vis. Sci.* **7**, 105–128 (2021).
13. Stasheff, S. F., Shankar, M. & Andrews, M. P. Developmental time course distinguishes changes in spontaneous and light-evoked retinal ganglion cell activity in rd1 and rd10 mice. *J. Neurophysiol.* **105**, 3002–9 (2011).
14. Morgans, C. W. Presynaptic proteins of ribbon synapses in the retina. *Microsc. Res. Tech.* **50**, 141–150 (2000).
15. Schmitz, F., Königstorfer, A. & Südhof, T. C. RIBEYE, a component of synaptic ribbons: a protein's journey through evolution provides insight into synaptic ribbon function. *Neuron* **28**, 857–872 (2000).
16. Lewis, G. P. & Fisher, S. K. Up-regulation of glial fibrillary acidic protein in response to retinal injury: its potential role in glial remodeling and a comparison to vimentin expression. *Int. Rev. Cytol.* **230**, 263–290 (2003).
17. Ortega, J. T. & Jastrzebska, B. Neuroinflammation as a Therapeutic Target in Retinitis Pigmentosa and Quercetin as Its Potential Modulator. *Pharmaceutics* **13**, (2021).
18. Yoshida, N. *et al.* Clinical Evidence of Sustained Chronic Inflammatory Reaction in Retinitis Pigmentosa. *Ophthalmology* **120**, 100–105 (2013).
19. Zhao, L. *et al.* Microglial phagocytosis of living photoreceptors contributes to inherited retinal degeneration. *EMBO Mol. Med.* **7**, 1179–1197 (2015).
20. Rashid, K., Akhtar-Schaefer, I. & Langmann, T. Microglia in Retinal Degeneration. *Front. Immunol.* **10**, 1975 (2019).
21. Wang, S. K., Xue, Y. & Cepko, C. L. Microglia modulation by TGF-β1 protects cones in mouse models of retinal degeneration. *J. Clin. Invest.* **130**, (2020).
22. Noailles, A. *et al.* Persistent inflammatory state after photoreceptor loss in an animal model of retinal degeneration. *Sci. Rep.* **6**, 33356 (2016).

23. Anishchenko, A. *et al.* Receptive field mosaics of retinal ganglion cells are established without visual experience. *J. Neurophysiol.* **103**, 1856–1864 (2010).

24. Field, G. D. *et al.* Functional connectivity in the retina at the resolution of photoreceptors. *Nature* **467**, 673–677 (2010).

25. Litke, A. M. M. *et al.* What does the eye tell the brain?: Development of a system for the large-scale recording of retinal output activity. *IEEE Trans. Nucl. Sci.* **51**, 1434–1440 (2004).

26. Chichilnisky, E. J. A simple white noise analysis of neuronal light responses. *Netw. Bristol Engl.* **12**, 199–213 (2001).

27. Keat, J., Reinagel, P., Reid, R. C. & Meister, M. Predicting every spike: a model for the responses of visual neurons. *Neuron* **30**, 803–817 (2001).

28. Marc, R. E. *et al.* Neural reprogramming in retinal degeneration. *Invest. Ophthalmol. Vis. Sci.* **48**, 3364–71 (2007).

29. Margolis, D. J., Newkirk, G., Euler, T. & Detwiler, P. B. Functional stability of retinal ganglion cells after degeneration-induced changes in synaptic input. *J. Neurosci. Off. J. Soc. Neurosci.* **28**, 6526–36 (2008).

30. Stasheff, S. F. Emergence of sustained spontaneous hyperactivity and temporary preservation of OFF responses in ganglion cells of the retinal degeneration (rd1) mouse. *J. Neurophysiol.* **99**, 1408–21 (2008).

31. Shannon, C. E. A Mathmatical Theory of Cummunication. *Bell Syst. Tech. J.* **27**, 379–423, 623–656 (1948).

32. McDonnell, M. D., Ikeda, S. & Manton, J. H. An introductory review of information theory in the context of computational neuroscience. *Biol. Cybern.* **105**, 55–70 (2011).

33. Nuzbrokh, Y., Ragi, S. D. & Tsang, S. H. Gene therapy for inherited retinal diseases. *Ann. Transl. Med.* **9**, 1278–1278 (2021).

34. Wagner, J. E. *et al.* In vivo potency testing of subretinal rAAV5.hCNGB1 gene therapy in the Cngb1 knockout mouse model of retinitis pigmentosa. *Hum. Gene Ther.* **32**, (2021).

35. Koch, S. *et al.* Gene therapy restores vision and delays degeneration in the CNGB1 2/2 mouse model of retinitis pigmentosa. *Hum. Mol. Genet.* **21**, 4486–4496 (2012).

36. Michalakis, S. *et al.* Gene therapy restores vision and delays degeneration in the CNGB1−/− mouse model of retinitis pigmentosa. *Adv. Exp. Med. Biol.* **801**, 733–739 (2014).

37. Petersen-Jones, S. M. *et al.* Patients and animal models of CNGβ1-deficient retinitis pigmentosa support gene augmentation approach. *J. Clin. Invest.* **128**, 190–206 (2018).

38. Koch, S. F. *et al.* Halting progressive neurodegeneration in advanced retinitis pigmentosa. *J. Clin. Invest.* **125**, 3704–3713 (2015).

39. Koch, S. F. *et al.* Genetic rescue models refute nonautonomous rod cell death in retinitis pigmentosa. *Proc. Natl. Acad. Sci. U. S. A.* 201615394 (2017) doi:10.1073/pnas.1615394114.

40. Nassisi, M. *et al.* CNGB1-related rod-cone dystrophy: A mutation review and update. *Hum. Mutat.* **42**, 641–666 (2021).

41. Chinskey, N. D., Besirli, C. G. & Zacks, D. N. Retinal cell death and current strategies in retinal neuroprotection. *Curr. Opin. Ophthalmol.* **25**, 228–233 (2014).

42. Léveillard, T. *et al.* Identification and characterization of rod-derived cone viability factor. *Nat. Genet.* **36**, 755–759 (2004).

43. Punzo, C., Xiong, W. & Cepko, C. L. Loss of Daylight Vision in Retinal Degeneration: Are Oxidative Stress and Metabolic Dysregulation to Blame? *J. Biol. Chem.* **287**, 1642–1648 (2012).

44. Hoy, J. L., Yavorska, I., Wehr, M. & Niell Correspondence, C. M. Vision Drives Accurate Approach Behavior during Prey Capture in Laboratory Mice. *Curr. Biol.* **26**, 3046–3052 (2016).

45. Shaw, L., Wang, K. H. & Mitchell, J. Fast prediction in marmoset reach-to-grasp movements for dynamic prey. 2022.10.08.511417 Preprint at https://doi.org/10.1101/2022.10.08.511417 (2022).

46. Poetsch, A., Molday, L. L. & Molday, R. S. The cGMP-gated Channel and Related Glutamic Acid-rich Proteins Interact with Peripherin-2 at the Rim Region of Rod Photoreceptor Disc Membranes*. *J. Biol. Chem.* **276**, 48009–48016 (2001).

47. Schindelin, J. *et al.* Fiji: an open-source platform for biological-image analysis. *Nat. Methods* **9**, 676–682 (2012).
48. Frechette, E. S. *et al.* Fidelity of the ensemble code for visual motion in primate retina. *J. Neurophysiol.* **94**, 119–135 (2005).
49. Yao, X. *et al.* Gap Junctions Contribute to Differential Light Adaptation across Direction-Selective Retinal Ganglion Cells. *Neuron* **100**, 216–228 (2018).
50. Field, G. D. *et al.* Spatial properties and functional organization of small bistratified ganglion cells in primate retina. *J. Neurosci. Off. J. Soc. Neurosci.* **27**, 13261–72 (2007).
51. Shlens, J. *et al.* The structure of multi-neuron firing patterns in primate retina. *J. Neurosci. Off. J. Soc. Neurosci.* **26**, 8254–8266 (2006).
52. Betsch, B. Y., Einhäuser, W., Körding, K. P. & König, P. The world from a cat's perspective - Statistics of natural videos. *Biol. Cybern.* **90**, 41–50 (2004).
53. *GoPro Awards: Squirrel Runs Off With GoPro*. (YouTube, 2016).
54. Strong, S. P., Koberle, R., De Ruyter Van Steveninck, R. R. & Bialek, W. Entropy and Information in Neural Spike Trains. *Phys. Rev. Lett.* **80**, 197 (1998).
55. Ma, S. keng. Calculation of entropy from data of motion. *J. Stat. Phys. 1981 262* **26**, 221–240 (1981).
56. Bates, D., Mächler, M., Bolker, B. M. & Walker, S. C. Fitting Linear Mixed-Effects Models Using lme4. *J. Stat. Softw.* **67**, 1–48 (2015).

Supplementary Figures

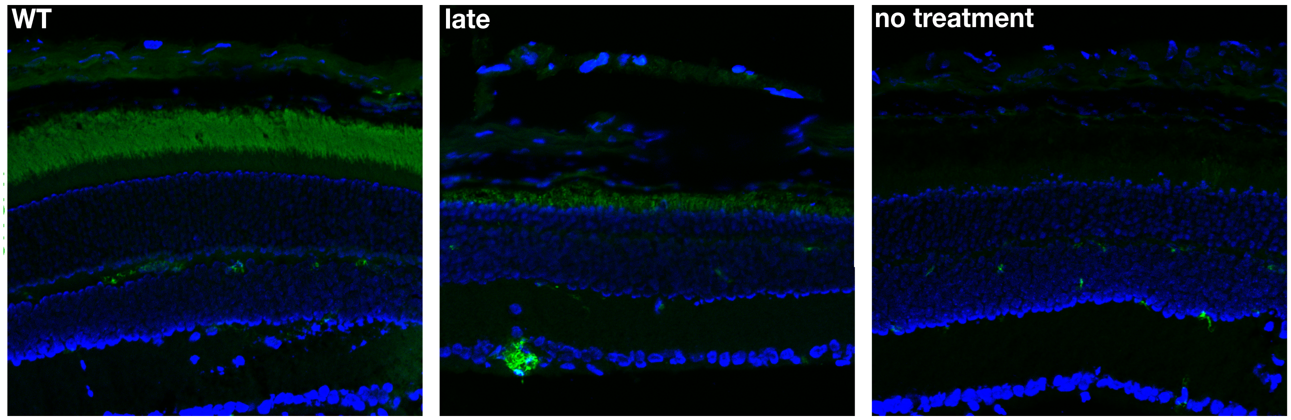


***Figure S1:* Cnga1 *expression is restored with late treatment.*** *Confocal images of retinal cryosections from WT, late treated* Cngb1$^{neo/neo}$ *mice, and untreated* Cngb1$^{neo/neo}$ *mice.* Cnga1 *expression in green and DAPI nuclei in blue. Similar results were obtained at earlier treatment timepoints.*

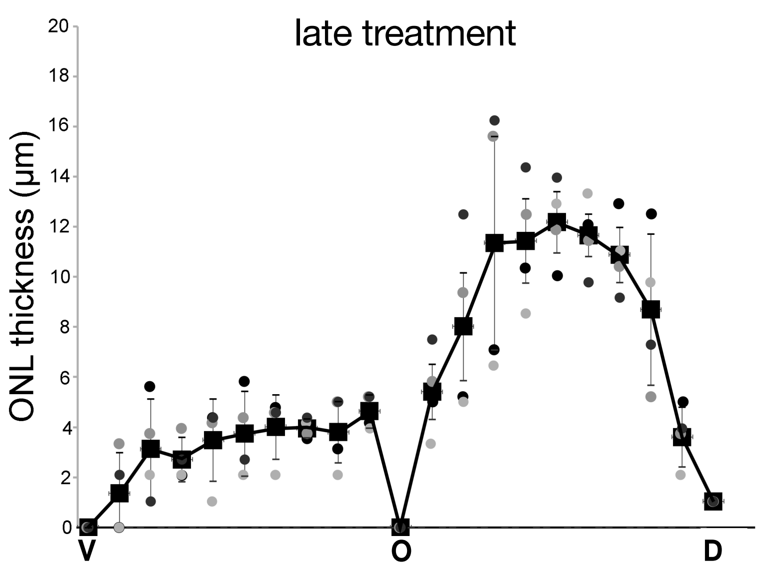


***Figure S2: Following late treatment, ventral photoreceptors are less preserved than dorsal.*** *Quantification of outer nuclear layer thickness from cross sections spanning dorsal to ventral retina. Each square is the average between two measurements (circles) taken from two retinas (grey and black). Qualitatively similar results were obtained at earlier treatment timepoints.*

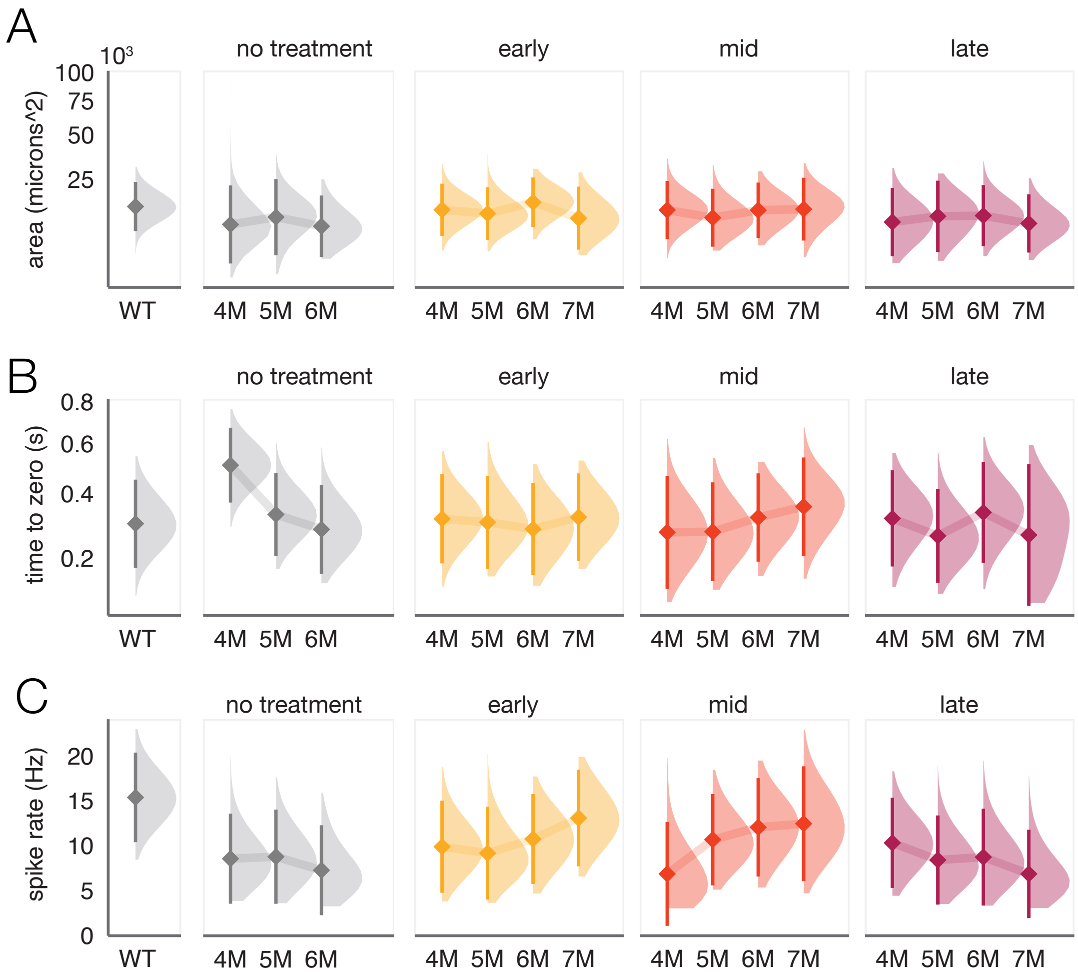


***Figure S3: Mesopic receptive field measurements are stable following treatment, but response gain under mesopic conditions does not recover following late treatment. Similar to Figure 4,*** *the panels show distributions of A) time to zero, B) receptive field size, and C) gain, (diamond is the mean and bar is +/- SD) in WT, untreated, early, mid and late treated retinas from 4 to 7M. Light level was 100 Rh*/rod/s.*

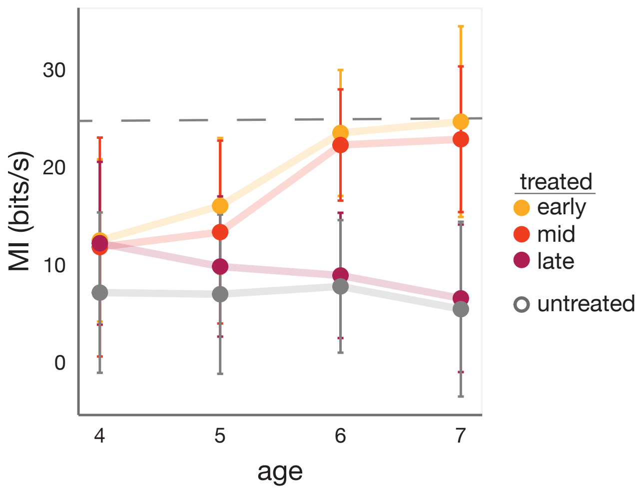


***Figure S4: Consistent with results at photopic and scotopic light levels, late treatment fails to restore RGC information rates in response to mesopic repeating checkerboard stimuli.*** *Mean +/- 2 SD mutual information rate of RGC responses (n = 2-6 retinas) at mesopic light level (100 Rh*/rod/s) from the 10% most informative RGCs. Dashed line indicates the mean information rate observed in RGC responses from WT retinas.*

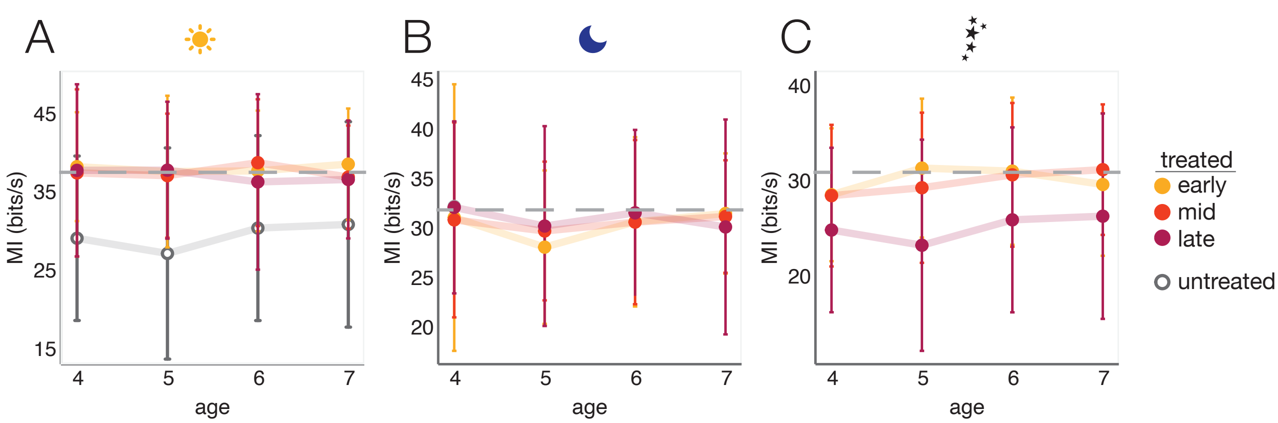


***Figure S5: RGC information rates in response to natural movies are higher and more robust to degeneration than checkerboard noise.*** *Following previous work (Scalabrino et al., 2022), we computed the median information rate for the 10% most informative RGCs. In untreated* Cngb1$^{neo/neo}$ *retinas, this population of RGCs exhibited the clearest changes in information rates compared to control retinas (Scalabrino et al.,2022). Consistent with this previous study, we observed that information rates were higher for natural movies than for checkerboard noise and less sensitive to rod photoreceptor loss. Correspondingly, for early, mid, and late treatment time points, RGC information rates for natural movies matched those of WT at all ages tested under photopic and mesopic conditions (A-B). However, under scotopic conditions, there was a reduction in the information rates at every age tested for the late treatment, but not for the early and mid treatment time points (C). In each panel, the points indicate the mean +/- 2 SD of the information rate of RGC responses (n = 2-6 retinas) from the 10% most informative RGCs. Dashed line indicates the mean information rate observed in RGC responses from WT retinas.*